



HAL
open science

Calibrating Resistance and Current Measurements in Conductive Probe Atomic Force Microscopy: New Reference Samples and Calibration Methods

François Piquemal, Pascal Chrétien, José Morán-meza, Frédéric Houzé, Alexandra Delvallée, Christian Ulysse, Abdelmounaim Harouri

► To cite this version:

François Piquemal, Pascal Chrétien, José Morán-meza, Frédéric Houzé, Alexandra Delvallée, et al.. Calibrating Resistance and Current Measurements in Conductive Probe Atomic Force Microscopy: New Reference Samples and Calibration Methods. *Physica Status Solidi A (applications and materials science)*, 2025, 10.1002/pssa.202400711 . hal-04922885

HAL Id: hal-04922885

<https://centralesupelec.hal.science/hal-04922885v1>

Submitted on 10 Feb 2025

HAL is a multi-disciplinary open access archive for the deposit and dissemination of scientific research documents, whether they are published or not. The documents may come from teaching and research institutions in France or abroad, or from public or private research centers.

L'archive ouverte pluridisciplinaire **HAL**, est destinée au dépôt et à la diffusion de documents scientifiques de niveau recherche, publiés ou non, émanant des établissements d'enseignement et de recherche français ou étrangers, des laboratoires publics ou privés.



Distributed under a Creative Commons Attribution - NonCommercial - NoDerivatives 4.0 International License

Calibrating Resistance and Current Measurements in Conductive Probe Atomic Force Microscopy: New Reference Samples and Calibration Methods

François Piquemal,* Pascal Chrétien, José Morán-Meza, Frédéric Houzé, Alexandra Delvallée, Christian Ulysse, and Abdelmounaim Harouri

Despite the considerable contributions of conductive probe atomic force microscopy (C-AFM) to the understanding of materials and devices' properties at the nanoscale, measurements remain prone to an arsenal of artifact-inducing factors. Herein, new calibration samples are developed enabling an easy access to highly accurate calibrated C-AFM measurements over expanded resistance and current ranges from 1 k Ω to 1 T Ω and from 10 fA to 10 μ A. For this purpose, the influence of the AFM probe (material, wear) is investigated by operating C-AFM in spectroscopy and imaging modes. Commendable measurement protocols are elaborated with associated simplified uncertainty budgets, showing that the combined standard uncertainties do not exceed a few percent over the whole resistance and current ranges. These calibration samples pave the way for reliable and reproducible quantitative measurements of resistance and current at the nanoscale, and the findings are expected to promote the adoption of the C-AFM for these nanoscale measurements.

functionality of these devices, conductive probe atomic force microscopy (C-AFM) is playing an increasingly important role in the characterizing and understanding of nanomaterials' and nanodevices' properties.^[1,2] Introduced in the early 1990s,^[3] C-AFM is based on applying a DC-bias voltage between a conductive AFM probe and a given sample in contact, enabling the surface topography mapping with a simultaneous collection of the current flowing through the tip/surface nanocontact. This operating principle unlocks two main C-AFM measurement approaches, i.e., mapping the local current variations over a scanned area (imaging mode), or collecting current versus voltage (I - V) curves at one specific point on the sample by sweeping the DC-bias voltage (spectroscopy mode).

However, the practical realization of such measurements is prone to two major difficulties. First, the current collected is likely to vary very rapidly over a considerable dynamic range, depending on the nature of the sample. Second, the measurement must be carried out at the AFM's operating rate. Despite various approaches and technical solutions proposed so far,^[1,4-8] nanoscale electrical measurements are still subject to numerous experimental challenges that can induce artifacts.^[9-12] These challenges have limited C-AFM measurements to qualitative comparisons in the majority of cases.

To overcome the aforementioned difficulties, a first wide-range multiresistance reference sample was recently proposed, as well as the basis for an associated operating procedure, enabling calibration of the complete C-AFM measurement circuit over a resistance range from 100 Ω to 100 G Ω .^[13] Nevertheless, the previously proposed sample still misses numerous aspects related to the full calibration of the resistance and current measurements. In this study, the development of new, more comprehensive reference samples and associated calibration methods is presented, with the aim of democratizing the calibration and reliability of C-AFM measurements.

The remainder of the article is organized as follows. Section 2 describes the sample's structure and its fabrication process using surface-mounted device (SMD) resistors. Moreover, it details the procedures for calibrating their resistances and current values at the macroscale using a probe station coupled with high precision voltage source and ammeter, as well as the associated uncertainty


1. Introduction

The development of nanoelectronic and quantum devices is fueling a frenetic need for calibrated, reproducible, and comparable measurements of electrical properties at the nanoscale. As measuring currents and resistances is key for elucidating the

F. Piquemal, J. Morán-Meza, A. Delvallée
Laboratoire national de métrologie et d'essais
29 Av Roger Hennequin, 78197 Trappes Cedex, France
E-mail: francois.piquemal@lne.fr

P. Chrétien, F. Houzé
Laboratoire de génie électrique et électronique de Paris - Université Paris-Saclay - CentraleSupélec - CNRS
11 Rue Joliot Curie, 91192 Gif-sur-Yvette, France

C. Ulysse, A. Harouri
Centre de nanosciences et de nanotechnologies - Université Paris-Saclay - CNRS
10 Bd Thomas Gobert, 91120 Palaiseau, France

 The ORCID identification number(s) for the author(s) of this article can be found under <https://doi.org/10.1002/pssa.202400711>.

© 2024 The Author(s). physica status solidi (a) applications and materials science published by Wiley-VCH GmbH. This is an open access article under the terms of the Creative Commons Attribution License, which permits use, distribution and reproduction in any medium, provided the original work is properly cited.

DOI: 10.1002/pssa.202400711

contributions. Then, Section 3 presents the calibration protocols elaborated for C-AFM systems, in both imaging and spectroscopy modes, with a summary of the main steps to be followed. In Section 4, the application of the developed samples and methodologies is demonstrated to a particular C-AFM configuration, based on an electrical measurement device referred to as wide-range current measuring device (WCMD). Finally, the conclusions and outlooks of this work are given in Section 5.

2. Reference Samples

2.1. Design and Fabrication

The new calibration samples (identified as type 4 A) consist of a squared fused silica substrate (11 mm wide, 2 mm thick), on which metallic connection lines and pads were fabricated (Figure 1).

The fabrication details are available elsewhere.^[13] Two sample batches were produced using two different metals (i.e., Au and Pt) for the electrodes. Pt features a lower affinity to contamination compared to Au. Each sample is composed of SMD resistors connected to microelectrodes covering the range between 1 k Ω and 1 T Ω . The new calibration samples feature a “short-circuit” electrode (SC in Figure 1) allowing a direct connection of the tip to the bias voltage source, enabling in situ measurements of the tip’s resistance. Moreover, the new samples are fitted with three other electrodes connected to an SMD junction field-effect transistor (JFET) diode (from InterFET) to enable the C-AFM DC current calibration. Each sample features 15 arms terminated by electrodes located in a 60 \times 60 μm central area, as shown in Figure 1. Owing to its different applications (i.e., calibration of C-AFM in terms of DC resistance, DC current, and in situ measurement of the tip’s resistance), the newly developed sample constitutes a comprehensive calibration kit for C-AFM.

2.2. Calibration

Two samples (Au and Pt electrodes) were calibrated using a four-probe station (Cascade Microtech MPS150 from FormFactor) coupled to a programmable voltage source (Marconi 104 A) and a

high-precision ammeter.^[13] The whole setup is located in an electromagnetically shielded environment under stabilized air temperature (typically, 23 $\text{^\circ C} \pm 0.1 \text{^\circ C}$) and relative humidity (RH) (typically, 40.0% \pm 0.3%). Two different calibrated ammeters were used depending on the range of the resistance or current values, i.e., a digital voltage multimeter (DVM) (Keysight 3458 A) typically for resistances below 1 G Ω , or a femtoampere current amplifier (Femto DDP-CA-300, see S1, Supporting Information) associated with the same DVM for resistance equal or larger than 1 G Ω (or for current ranging from 1 fA to 1 μA).

The setup contributes in the uncertainty budget corresponding to resistance measurements at a level between 1.3 parts in 10⁴ (100 Ω) and 1.3 parts in 10³ (1 T Ω). The main uncertainty components are due to gain calibration, leakage resistances, and measurement noise.^[13] For current measurements, the uncertainty due to the setup varies between 2.6 parts in 10³ (10 fA) and 6.9 parts in 10⁴ (1 μA). All the uncertainties reported in the article are given at 1 standard deviation which corresponds to a 68% confidence level in the case of a normal distribution.^[14]

2.2.1. Resistance Calibration for the Ten Arms with SMD Resistors

The resistance of the ten complete arms from the electrode (central area, Figure 1c) to the peripheral track (in brown, Figure 1b) connected to the back electrode has been measured in two steps. First, the resistance is measured between the intermediate pads (in brown, Figure 1b) and the back electrode by applying the two-terminal method for the arms with resistance larger than 1 k Ω and the four-terminal method for the arm without SMD resistor and the arm connected to 1 k Ω SMD resistor. Using the resistance measurement of the arm without SMD resistor, the resistivity of the line is calculated based on its dimensional parameters (width, thickness, and length).^[13] Second, the resistivity values and the dimensional parameters are used to calculate the resistance of the line segment from the electrode to the intermediate pad (not measurable by the probe station). Table S2, Supporting Information, reports the calibrated resistance values, the resistance of the line segments, and the measured resistivity for Au and Pt.

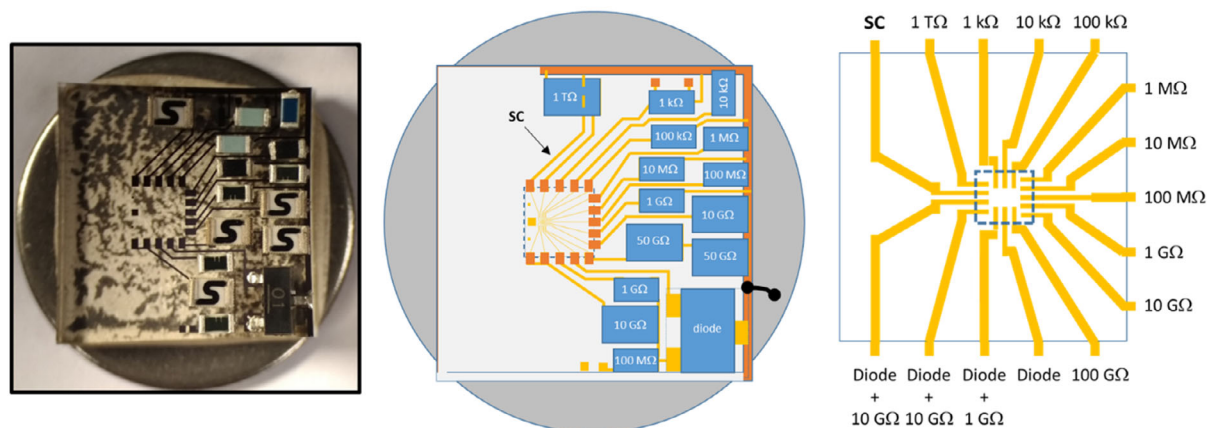


Figure 1. (Left) Picture of the new calibration sample (type 4 A) composed of SMD resistors and JFET-based diode; (middle and right) drawings showing the implantation of SMD resistors covering the resistance range between 1 k Ω and 1 T Ω . The central area (60 \times 60 μm) for AFM scan is indicated with a blue dashed rectangle (right). The intermediate pads and peripheral track (orange) are used for probe-station measurements, the peripheral track being connected to the back electrode (circular metallic holder). One arm (passing underneath the 1 T Ω resistor) is used as short circuit (SC).

Table S3, Supporting Information, summarizes the uncertainty contributions associated with the resistance values provided by these new reference samples, including the setup uncertainty, measurement noise, and uncertainties related to the SMD resistors' parameters. Applying the root sum square (RSS) method on these uncertainties results in combined total uncertainty ranging from $6.9 \cdot 10^{-4}$ for the smallest resistance values up to $2.3 \cdot 10^{-3}$ for the highest ones.

Furthermore, the uncertainties related to the temperature and voltage effects on the SMD resistors were evaluated taking into account the manufacturer specifications. The uncertainties associated with the RH effect were estimated from resistance measurements carried out with RH values varying between 43.2% and 58.0%. It is worth noting that the stability of the SMD resistors' resistance has been investigated for a period of 6 months. No drift has been observed within 0.1% for the whole resistance range, leading to an uncertainty less than $6 \cdot 10^{-4}$ in the worst case.

It must be noted that the combined total uncertainty (Table S3, Supporting Information) will intervene in the uncertainty budget corresponding to the calibration of C-AFM in terms of resistance without any change if the environmental conditions (temperature, RH) remain unchanged. The same budget remains valid for the calibration of C-AFM in terms of current by applying a known voltage to the SMD resistors (Table S4, Supporting Information).

2.2.2. Current Calibration for SMD JFET Diode

The current generated by the SMD JFET diode (Pt electrodes sample) by sweeping the bias voltage from 0 V up to 0.7 V

has been measured by changing successively the transimpedance gain of the current amplifier from 10^{13} V A^{-1} up to 10^6 V A^{-1} (Figure 2a). The resulting I - V curves have been superimposed, taking into account both the calibrated gain values and the measured offset input current of the amplifier, and then averaged to determine the calibration I - V curve (Figure 2b). Thus, this calibration curve covers a much expanded current range from a few femtoamperes to $10 \mu\text{A}$ with reduced standard deviation of the data distribution due to good overlaps of I - V curves recorded with different transimpedance gains.

The calibration curve was successfully fitted with a third-order polynomial (Figure 2c)

$$I_{\text{fit}} = I_0 \exp(b_1 V + b_2 V^2 + b_3 V^3) \quad (1)$$

with the following parameters: $I_0 = (142.10 \pm 0.09) \text{ aA}$, $b_1 = (28.25 \pm 0.23) \text{ V}^{-1}$, $b_2 = (21.15 \pm 0.64) \text{ V}^{-2}$, and $b_3 = (-15.17 \pm 0.53) \text{ V}^{-3}$.

It has been found unnecessary to push the fit at orders larger than 3 to get fit values agreeing with the measured values within about $\pm 5\%$ over the full voltage range (Figure 2c).

Assuming that $b_1 = e/(\eta kT)$, where e is the electron charge and k is the Boltzmann's constant, leads to find an ideality factor $\eta = 1.403 \pm 0.011$ which is consistent with expected values (typically between 1 and 2) for tunnel junction-based devices.

From relations giving these parameters, a low influence of the voltage source resolution on the measurement's accuracy is expected. Indeed, a voltage error as large as 1 mV will yield a small relative error $\Delta I/I$ not exceeding +0.4% over the full voltage range.

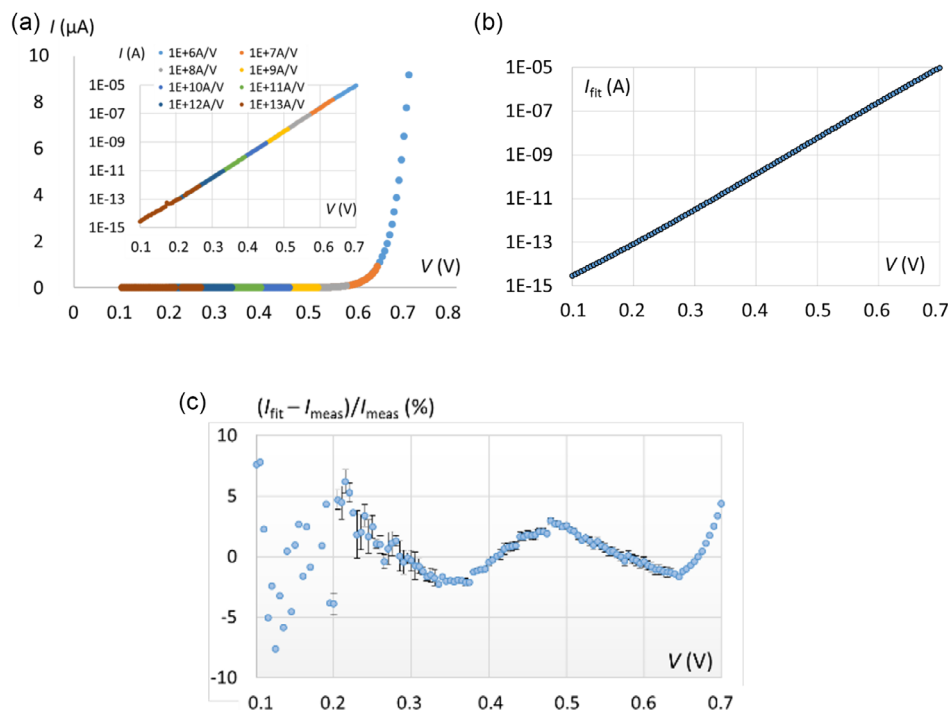


Figure 2. a) I - V curves in linear or semilog (insert) scale measured on the Pt electrodes sample using the electrode connected directly to the SMD diode (pad#10). b) Mean current values (calculated from I - V curves recorded with different gains for the same current range) versus voltage. c) Relative deviation between the fit values and the mean values using third-order polynomial.

The temperature dependence of the current delivered by the JFET diode of the Pt electrodes sample in this case has been evaluated by performing measurements on another JFET diode provided from the same batch. This diode was placed inside an ultrastable temperature chamber (type TK-190-US from Kambic) and I - V curves were measured at three temperatures, 21 °C, 23 °C, and 25 °C, using the same measurement setup. It results in the following temperature coefficients associated with parameters b_1 , b_2 , and b_3

$$a_{T,b1} = (0.876 \pm 0.002)V^{-1}/K \quad (2)$$

$$a_{T,b2} = (-2.123 \pm 0.006)V^{-2}/K \quad (3)$$

$$a_{T,b3} = (1.462 \pm 0.004)V^{-3}/K \quad (4)$$

Considering these values, the error on the current delivered by the diode is far to be negligible. The relative error amounts to $9 \cdot 10^{-3}$ if the temperature deviates by 0.1 °C from the calibration temperature (typically 23 °C).

The complete uncertainty budget associated with the calibration of the I - V curve provided by the JFET diode is detailed in Table S5, Supporting Information. Four uncertainty components are considered, giving rise to a total uncertainty ranging between 1.0% (10 fA) and 0.4% (1 μ A) as calculated by the RSS method. The first uncertainty component is related to the calibration setup. It combines the calibration uncertainty of the setup itself and the uncertainty estimated from the noise spectrum of the current amplifier for a typical measurement time of 80 s. The second uncertainty component is due to the temperature dependence of the JFET diode. The uncertainty is estimated in this case from a rectangular distribution centered at $23.0 \text{ °C} \pm 0.1 \text{ °C}$, assuming that the error is not corrected. The last uncertainty component reflects the reproducibility of the I - V curve delivered by the JFET diode. Measurements performed over 5 days do not show any time drift on the current within the measurement uncertainty. As a precaution, a conservative value of 0.1% is considered for this uncertainty.

Instead of using the calibrated I - V curve obtained from the JFET diode, it would be preferred, for simplicity, to consider the polynomial fit of third order to calculate the current for a given voltage. In this case, the calibration uncertainty is estimated at 2.9% for the whole 10 fA to 1 μ A range, the fit agreeing within $\pm 5\%$ with the measured values. Accordingly, it becomes the major uncertainty component.

3. Calibration Procedures

3.1. Calibration of C-AFM for Resistance Measurements

The calibration protocol summarized here is applied for C-AFM operating in spectroscopy (I - V) and imaging modes; it was developed considering two types of tip coatings (PtSi and doped diamond) and consists of five steps (Figure 3). Much more details of this protocol are given in Section 6. The first two steps are common for both modes.

Step 1 consists in eliminating any possible contamination of the tip apex by repeatedly scanning over a fixed scan line (typically a length of few tens of nanometers) on the sample surface

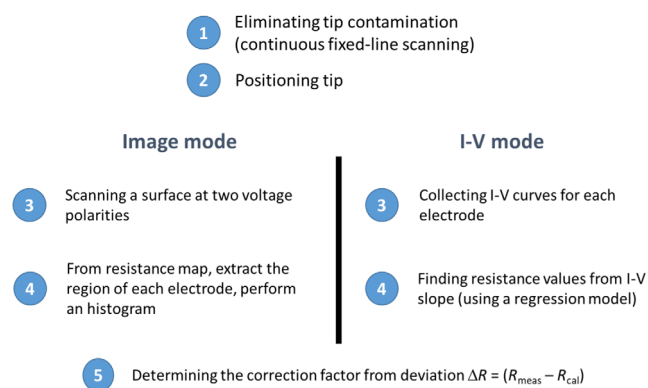


Figure 3. C-AFM calibration procedure for resistance measurements.

(i.e., by disabling the slow scan axis). The effective contamination removal was associated with a stable measurement of a minimal resistance value.

As second step, the AFM tip is positioned at a fixed location in contact with the electrode surface with a constant applied force, here 1.5 μ N for PtSi-coated tip and 3.0 μ N for doped diamond-coated tip.

The third step corresponds to the measurement itself. For spectroscopy mode, I - V curves are extracted by sweeping the applied voltage between, typically -1 V and $+1$ V. For the image mode, either a surface of $60 \times 60 \mu\text{m}$ embracing all the resistive electrodes or partial images of group of electrodes are scanned, by applying a constant bias voltage, typically $V_{in} = +1$ V. Then, the scan is repeated with the reversed polarity of the bias voltage, i.e., $V_{in} = -1$ V. The use of the two polarities (i.e., ± 1 V) is mandatory when the C-AFM is fitted with a highly doped diamond-coated tip for which a photoconductive effect was observed^[13] (for the rationale behind this statement, refer to Section 4.2.3).

In the fourth step, the measured resistance values R_{meas} are determined, either from I - V slope by applying a regression model on the data in the spectroscopy mode, or, in the image mode, by extracting the region of each electrode from resistance map, and then by performing an histogram and fitting data to log-normal distribution. The uncertainty corresponding to found resistance values is given by the standard deviation of the data fits (normal distribution). In the spectroscopy mode, the standard deviation can be calculated either from the regression method applied on a single I - V curve or from several I - V curves (by repeating the third step).

The last step, common to both modes, consists in comparing R_{meas} values against the calibrated resistance values R_{cal} and determining the correction factor to apply to C-AFM reading system. Optionally, the process can be repeated to check the agreement with R_{cal} values.

3.2. Calibration of C-AFM for Current Measurements

There are two approaches to calibrate C-AFM for current measurements in both spectroscopy and image modes. The first approach involves the SMD resistors while the second one uses the SMD JFET diode.

3.2.1. SMD Resistors

By scanning the AFM tip successively on each resistive electrodes, the current range can be covered over 10 decades but in discrete values (e.g., applying $V_{in} = 1$ V on resistive electrodes which have resistances of 1 T Ω , 1 G Ω , and 1 M Ω , the delivered current values will be: 1 pA, 1 nA, and 1 μ A).

The calibration procedure described above (Figure 3) remains unchanged for C-AFM operating in image mode, except for the fourth step dealing with DC current map and the last step which compares measured current values, I_{meas} , against calibrated current values I_{cal} (Figure 4a).

For the spectroscopy mode, only the third step and fourth step are changed. For each electrode, the current measurement consists in periodically reversing the polarity of the applied voltage V_{in} , for example, $V_{in}^- = -1$ V, then $V_{in}^+ = +1$ V giving rise to two current values I^- and I^+ , and then repeating this cycle several times, typically ten times. In the fourth step, the mean current value is extracted by averaging the n data $\langle I_j \rangle = (I_j^+ - I_j^-)/2$ with j varying from 1 to n and calculating the corresponding standard deviation.

3.2.2. SMD JFET Diode

In spectroscopy mode, the AFM tip being in contact to the surface of the electrode electrically connected to the SMD JFET diode (electrode #10); sweeping the voltage from 0.1 V up to 0.7 V enables to calibrate the C-AFM over continuous current values ranging from 10 fA up to 100 μ A. In image mode, repeating a scan of a defined area of the electrode at different voltages allows to provide a calibration of C-AFM for any current value of interest in the same range (10 fA–100 μ A). It is worth mentioning here that possible voltage shift can occur with the use of highly doped diamond-coated tip due to photoconductive effect, which creates a significant error, much larger than 10% in relative value. Then, it is highly recommended either to determine the voltage shift by carrying out I – V curve on electrode connected to a SMD resistor, or to use metallic tip (PtSi, CrPt, etc.).

Figure 4b gives the scheme of the calibration procedure, with first two steps unchanged. In the third step, for the spectroscopy mode, the bias voltage is swept from 0.1 V up to 0.7 V by constant voltage increments, which provide the current values desired by

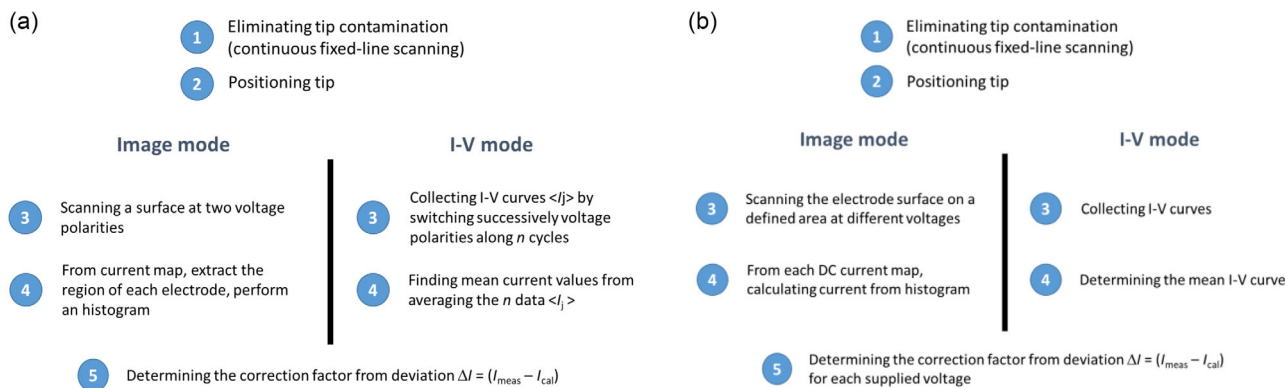


Figure 4. C-AFM calibration procedure for current measurements a) with SMD resistors or b) with SMD JFET diode.

the user. Care has to be taken on the voltage sweeping speed, which must be compatible with the bandwidth of the current amplifier used. Repeating at least three times the I – V curves is recommended to estimate the standard deviation of the data distribution associated with the calibrated I – V curve (step 4). For the image mode, the third step consists in repeating the scan of the AFM tip on a defined area of the electrode at different voltages. In the fourth step, the current value is calculated by performing an histogram and fitting data to Gaussian distribution. Then, the correction factor is determined from deviation $\Delta I = (I_{meas} - I_{cal})$ at each voltage value (fifth step).

4. Applications

4.1. C-AFM Setup

The C-AFM setup chosen to be calibrated here with these new reference samples relies on an electrical measurement device called WCMD. This device uses a Multimode 8 AFM system with a Nanoscope V controller (Bruker, USA) to obtain real-time maps of current or resistance, as well as I – V curves over a range of more than 11 decades (Figure 5).

The principle of the measurement is to apply a DC voltage to the sample and continuously read the current flowing through the tip and the sample at each point on the surface to be analyzed.

It is then possible to construct, point by point, an electrical image in parallel with the topographical AFM image.

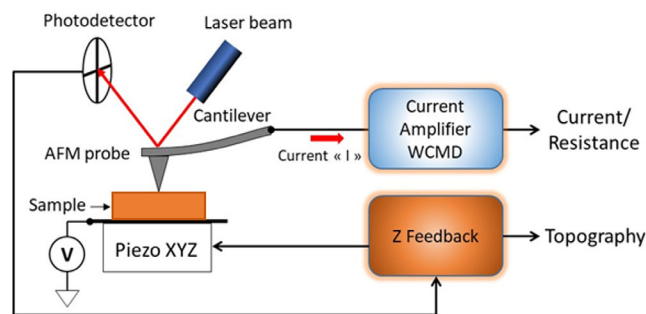


Figure 5. Schematics of the C-AFM operating with a WCMD current amplifier.

The high dynamic range of the WCMD requires the use of a voltage scale proportional to the decimal logarithm of the current ($\log(I)$) or resistance ($\log(R)$).

At its design stage, the device was calibrated using commercial reference resistors with a tolerance of less than 1%.

The measurement rate is a few tens of kilohertz with a bandwidth of 3 kHz. The measurable current range varies from a few tens of femtoamperes to a few milliamperes. For the smallest currents, transimpedance is 10^9 A V^{-1} and RMS noise estimated is 800 μV over a frequency band of 10 kHz.

4.2. Calibration Results for Resistance Measurements

Applying the procedures previously described, the C-AFM was calibrated in terms of resistance using the two samples (Au and Pt electrodes) as reference standards. The C-AFM was operated in spectroscopy and image modes, the AFM tip being in permanent contact to the sample surface.

4.2.1. Spectroscopy Mode

I - V curve measurements were performed with the C-AFM using two kinds of tip, PtSi-coated tip and highly doped diamond-coated tip. For each electrode of the sample, a set of five to nine I - V curves were recorded. For example, **Figure 6** shows the I - V curves measured on three Au electrodes of the reference sample using PtSi-coated tip: electrodes #1 (1 k Ω), #5 (10 M Ω), and #15 (1 T Ω). For most of the electrodes, the sets of I - V curves look like those observed for electrode #5 and for them a single I - V curve is enough to extract the resistance value by applying a linear regression model. Thus, for electrode #5, the mean resistance values from the six curves and that derived from regression model were

found in very good agreement within $1 \cdot 10^{-4}$ with relative standard deviations of $4.47 \cdot 10^{-5}$ and $4.55 \cdot 10^{-5}$, respectively. In the case of electrode #15 (1 T Ω), a good agreement was also found within 4×10^{-3} , with standard deviations of $2.5 \cdot 10^{-3}$ and $1.5 \cdot 10^{-3}$ calculated from the set of I - V curves and from the regression model applied on a single curve (Table S6a, Supporting Information).

However, for electrode #1 (1 k Ω), it was found really necessary to repeat several times the I - V curve measurements since a drift was observed until a stabilization of the resistance (Figure 6d).

Table S6b,c, Supporting Information, report the measured resistance values on all Au electrodes sample and Pt electrodes sample, respectively, including the standard deviation associated with the data distribution and the combined uncertainty. The latter is calculated from the RSS of the standard deviation, the uncertainty related to the calibration of the reference sample, and the uncertainty related to the tip resistance measurements. As shown in these tables, the standard deviations are typically lower than 0.1% for resistances ranging from 1 M Ω to 100 G Ω and remain lower than 0.3% for 1 T Ω . Therefore, these standard deviations are lower than the calibration uncertainty of the reference sample. However, for resistance value lower than 1 M Ω , the standard deviation can become the major uncertainty, reaching a few percent or even larger (as shown in Figure 6).

Figure 7 shows calibration results from these I - V curves in the form of relative deviations between measured and calibrated values for each resistive electrode of the two samples. For resistance ranging from 100 k Ω up to 100 G Ω , a very good agreement between measured values and calibrated ones has been found within $\pm 1\%$ independent of tip and electrode materials (Au or Pt). For highest resistance values (1 T Ω), the significant deviations remain lower than 9% and they are mainly due to the measurement uncertainty itself. For resistances equal or lower than 100 k Ω , significant deviations only occur when using

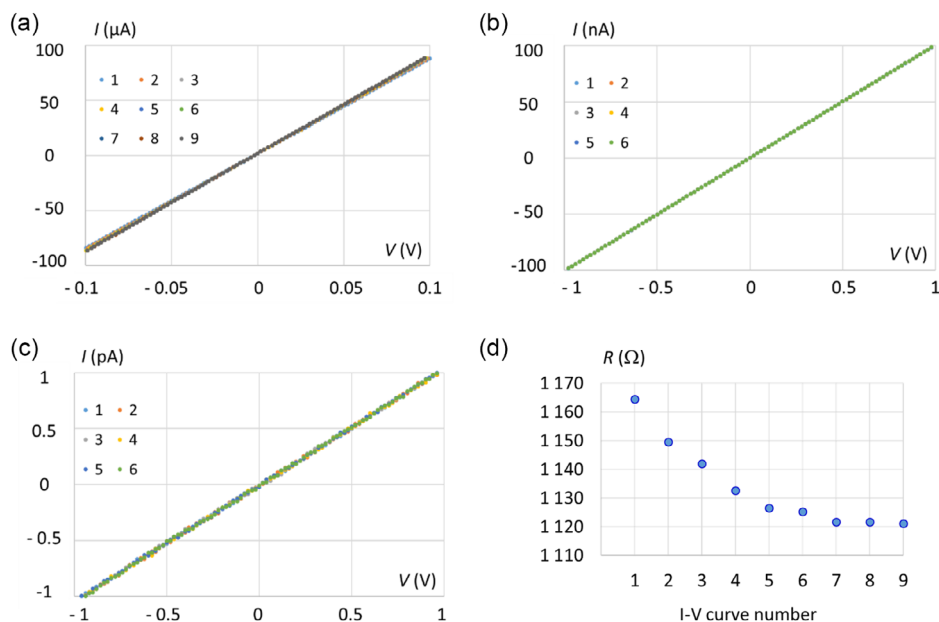


Figure 6. Typical I - V curves measured on Au electrodes reference sample. Here, C-AFM was fitted with PtSi tip: a) nine datasets measured on electrode #1 (1 k Ω); b) six datasets on electrode #5 (10 M Ω); c) 6 datasets on electrode #15 (1 T Ω); and d) resistance values extracted from I - V curves measured on electrode #1 with standard deviations in the order of 0.3–0.4 Ω .

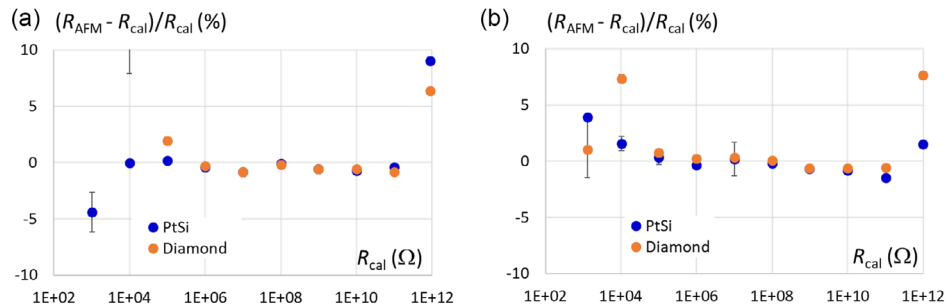


Figure 7. Relative deviations of measured resistance values and calibrated ones for each resistive electrode of two samples: a) Au electrodes sample and b) Pt electrodes sample. Two tips have been used, PtSi (blue full circle) and doped diamond-coated tip (orange full circle).

diamond-coated tip due to its resistance, in the order of 10 k Ω , in contrast with less resistive PtSi tip (in the order of few hundred ohms). The results shown in Figure 7 were corrected from tip resistance.

Error bars in Figure 7 are calculated by the RSS method applied on three uncertainties: the standard deviation of data (Table S6b,c, Supporting Information), the uncertainty related to the calibration of the sample (Table S3, Supporting Information), and the uncertainty corresponding to the tip resistance (only for $R < 1$ M Ω).

4.2.2. Image Mode

The calibration of the C-AFM operating in image mode was performed on the same two reference samples.

Au Electrodes Sample: To check the reproducibility of the C-AFM calibration and to investigate the possible influence of the tip coatings, measurements were performed on the Au electrodes sample with PtSi-coated tip and highly doped diamond-coated tip. Three complete images of the overall electrodes as shown in Figure 8 (over $60 \times 60 \mu\text{m}$) were recorded at both voltage polarities +1 V and -1 V.

To calculate the resistance measured on each electrode, a histogram was extracted from a rectangular portion of image with a larger area of $5.1 \times 10 \mu\text{m}$, covering entirely the electrode on the width, i.e., including the edges of the electrode. Figure 9 presents three typical histograms measured at +1 V on the electrodes #2 (10 k Ω), #6 (100 M Ω), and #9 (100 G Ω) for the two kinds of tip. For resistances $R \geq 1$ M Ω , the data follow relatively well a log-normal distribution (e.g., electrode #6) but with an unexpected distribution tail occurring before the peak for resistances larger than 1 G Ω (e.g., electrode #9). This effect originates from the excess noise due to WCMD electronics relatively to the signal of resistance to be measured. The influence of the tip on the measurements is clearly visible for smaller resistances ($R < 1$ M Ω) on the position of the peak and its shape (e.g., electrode #2), much more rounded with doped diamond tip. However, what they have in common is the asymmetry of the peak which can make it more difficult to estimate the resistance value.

As mentioned above (Section 3.1), for each extracted histogram, the peak resistance value and associated standard deviation are determined by fitting data to log-normal distribution. Systematically for a given electrode, two images are measured

by scanning the tip back and forth (usually named “trace” and “retrace”) and for each voltage polarities (here, +1 V and -1 V). The weighted mean value is then calculated from the four peak values and the corresponding standard deviations to give the final result (Table S7, Supporting Information).

Figure 10 shows the relative deviations calculated for each resistive electrode of the Au electrodes sample between the measured value and the calibrated value. The error bars correspond to the standard deviations of the weighted means. Independently of the kind of tip used (PtSi or doped diamond), very good agreements at the level of $\pm 2\%$ were observed between measured values and reference values for resistance ranging from 1 M Ω to 100 G Ω . In contrast with results obtained in spectroscopic mode, here all the standard deviations associated with the measured resistance values exceed a few tenths of a percent. They can reach a few percent in the resistance range between 1 M Ω and 100 G Ω , and even larger for the lower and upper resistance values (Table S7, Supporting Information).

A slightly lower dispersion on the relative deviations $(R_{AFM} - R_{cal})/R_{cal}$ was obtained with diamond-coated tip for resistances ranging from 1 M Ω to 100 G Ω . However, it was no more the case for the resistances equal or smaller than 100 k Ω . For this lower resistance range, similar to results obtained from I - V mode, the use of PtSi tip makes the C-AFM calibration possible. The calibrated values were found close to the reference values, i.e., within the interval $[-2\%, +5\%]$. On the contrary, the use of diamond-coated tip leads images with too large data distribution and makes difficult to estimate a mean value with relevant standard deviation (Figure 10).

Pt Electrodes Sample: Further measurements were carried out on Pt electrodes sample by C-AFM in image mode, again using tips coated with the two materials PtSi and doped diamond. The aim was twofold. First, it was necessary to investigate the influence of platinum compared with gold on the quality of images. As shown in Figure 11, very nice contrasts were observed with colors that match well the expected resistance values.

The aim was also to test a new measurement protocol which preserves the qualities of the tip during the scan and maximizes the chances of achieving a precise determination of the peak resistance values, in particular for the electrodes with smaller resistances ($R \leq 100$ k Ω). The qualities of the tip, especially in the case of a metallic coating, can deteriorate over the course of the measurements, so it is important to try to minimize the duration of these.

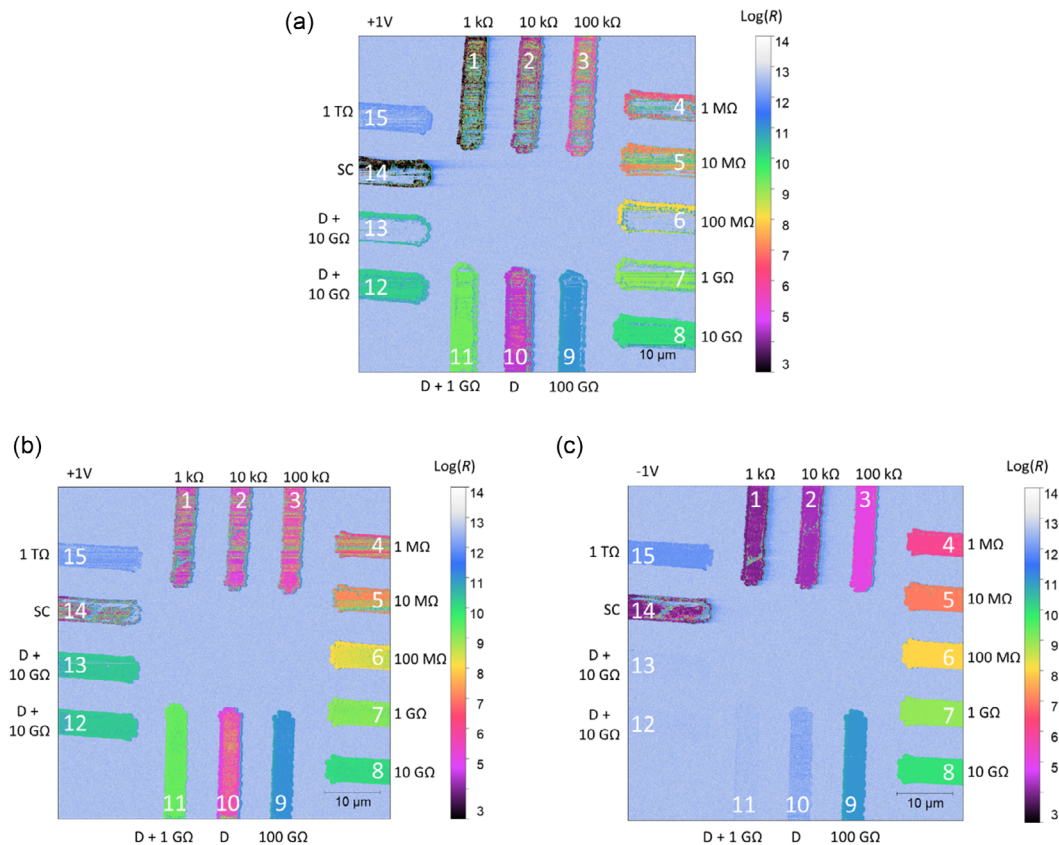


Figure 8. Resistance map (in decimal logarithm scale) of the central zone of the Au electrodes sample measured with C-AFM fitted with PtSi tip a) at +1 V and doped diamond coated tip at b) +1 V and c) –1 V. Numbers refer to the index i of the 15 electrodes. The electrode #10 is connected to the diode alone. The electrode #11 is connected to the diode in series with a 1 G Ω resistor. The electrodes #12 and #13 are connected to the diode in series with the same 10 G Ω resistor. The electrode #14 corresponds to the so-called “short circuit”.

The principle of this new protocol is to cover several electrodes (not all at once), to ensure that the tip is in the same state for the electrodes concerned and to take half an image for each voltage polarization.

Measurements were then performed by covering all the electrodes with four zones: zone #1, 14-1-2-3; zone #2, 4-5-6-7-8; zone #3, 9; and zone #4, 14-15. So only electrode #9 was imaged separately (Figure 12). The scan size was adapted according to the zone.

As for Au electrodes sample, the same process was used to determine the resistance values and associated standard deviations (extract histogram by considering the full width of the electrode, including edges, and the maximum possible length along the electrode axis; fit data to log-normal distribution; calculate weighted mean value from the four peak fitted values).

The measured resistance values and the associated standard deviations are given in Table S8, Supporting Information.

Figure 13 reports the relative deviations calculated for each resistive electrode of the Pt electrodes sample between the measured value and the calibrated value. The values measured on resistance electrodes from #2 (10 k Ω) to #8 (10 G Ω) agree very well, within $\pm 1\%$, with calibrated values. The measured values for the electrodes #1 (1 k Ω), #9 (100 G Ω), and #15 (1 T Ω) are also found consistent with the calibrated values considering the associated standard deviations.

Compared with the results obtained on Au electrodes sample (Figure 10), a slightly better agreement was found with Pt electrodes sample on the whole resistance range, independently of the tip coating material (PtSi or doped diamond).

4.2.3. Photoconductive Effect

As we mentioned in a previous paper^[13] which presented very first results on a reference sample of the previous generation, it appears that the I – V curves obtained with doped diamond-coated tips do not pass through zero. In the aforementioned publication, it was assumed that the offset currents observed at zero bias were associated with a photovoltaic effect involving the doped silicon of the tip core, which would have been locally exposed to the illumination of the AFM laser beam following wear of the tip apex. This was confirmed just afterward, i.e., after the article^[13] was published, by an image of this tip taken from scanning electron microscopy (SEM, Zeiss, Ultra Plus) as shown in Figure 14.

After numerous new series of tests, hindsight now suggests to refine our hypothesis and assume, rather than tip wear, a greater or lesser opacity of the doped diamond coatings. Indeed, the offset phenomenon has since been observed with several new tips.

To illustrate the photoconductive effect observed with doped diamond-coated tips, Figure 15 shows two typical I – V curves

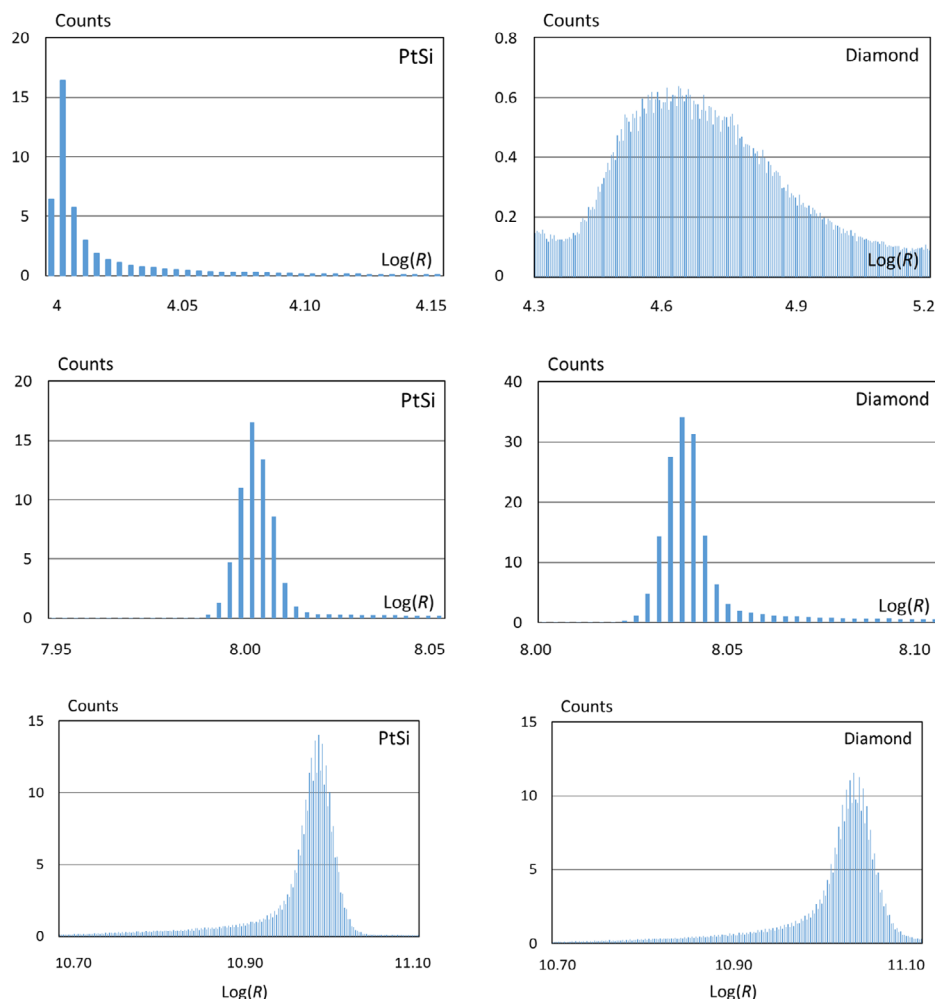


Figure 9. Associated histogram of data for measurements performed with PtSi-coated tip (left) and doped diamond coated tip (right) at +1 V on: electrode #2—10 kΩ (top); electrode #6—100 MΩ (middle); and electrode #9—100 GΩ (bottom).

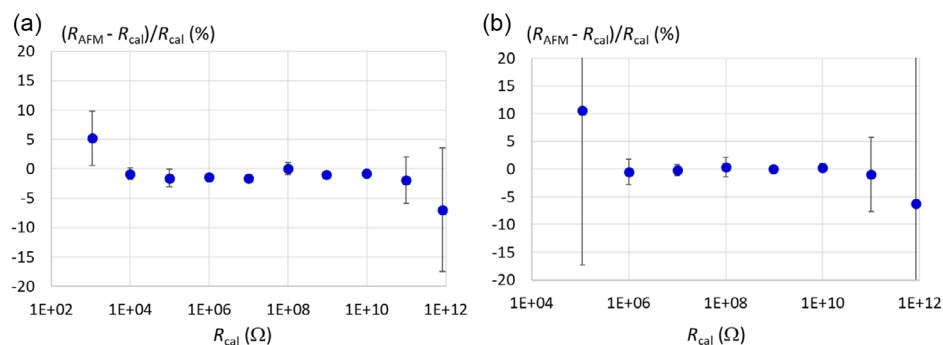


Figure 10. Relative deviations of measured resistance values and calibrated ones for each electrode of the same Au electrodes sample imaged using a) PtSi tip and b) doped diamond-coated tip. The error bars correspond to the standard deviations.

obtained on electrode #4 (1 MΩ) of the Au electrodes sample, with the AFM laser beam on (red curve) and without it (blue curve). These measurements were made with the same tip and carried out successively, so the tip showed the same degree

of usage. It is important to note that simply moving the laser beam along the cantilever away from the tip is not enough to eliminate the effect, as the entire probe (tip + lever) is sensitive to the effect of the laser light. So the blue curve was obtained by

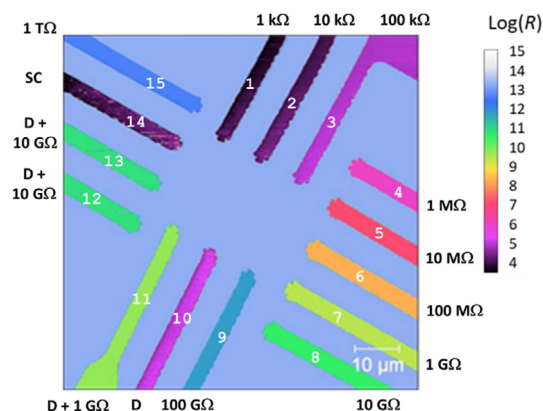


Figure 11. Resistance map of the central zone of the Pt electrodes sample scanned with a doped diamond coated tip at +1 V.

physically switching off the laser beam for the short time needed to record the curve. It can be seen that the current measured at zero polarization is 40 times higher in the presence of the laser beam than in its absence. However, whether the laser is switched on or off, the $I-V$ curves are perfectly linear, with extremely close slope values. The same findings were reproduced for other electrodes of the same sample.

Figure 16 shows the different $I_{\text{offset}} \times R_i$ products measured with different tips during the $I-V$ measurement campaigns on the two samples (Au and Pt electrodes), two of each with tips from two different batches. The values appear to fall into two groups, with the largest absolute values around 80 mV relating to the Au electrodes sample and similar to that observed in ref. [13] using another diamond-coated tip (coming from a third batch) with the former reference sample also fitted with Au electrodes. This might suggest that the diamond coating on the tip

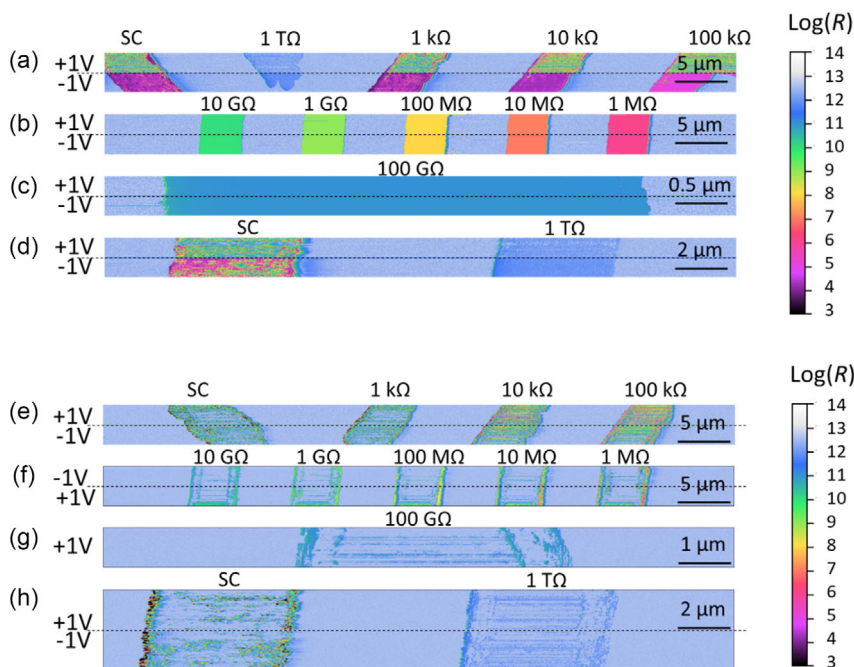


Figure 12. Resistance map of four zones of the Pt electrodes sample scanned with a,b,c,d) a doped diamond-coated tip and e,f,g,h) a PtSi-coated tip.

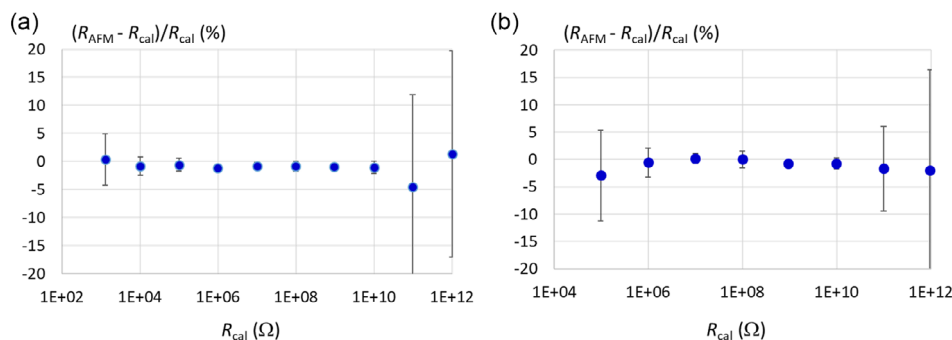


Figure 13. Relative deviations of measured resistance values and calibrated ones for each resistive electrode of the same Pt electrodes sample imaged using a) PtSi tip and b) doped diamond-coated tip. The error bars correspond to the standard deviations.

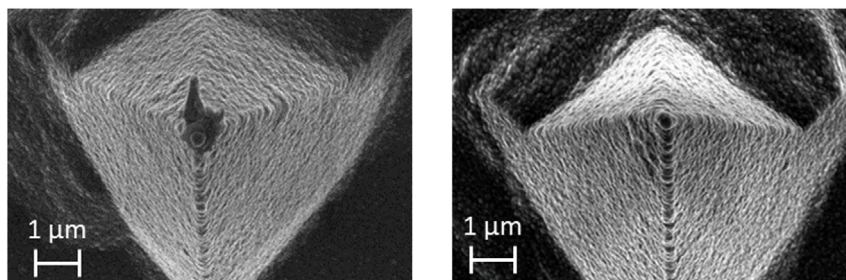


Figure 14. (Left) SEM image of the diamond-coated tip showing a tearing of the coating at the end of the tip. This image was taken after the measurements reported in ref. [13]; (right) image of the same kind of tip but not used.

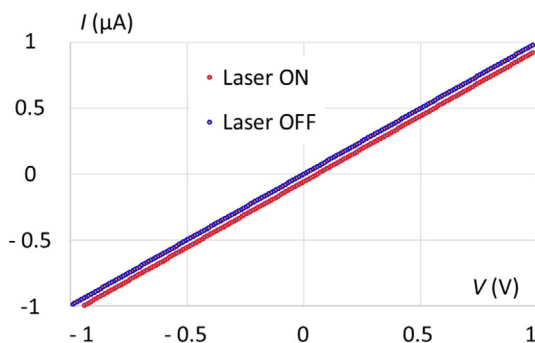


Figure 15. I - V curve measured on Au electrode #4 ($1\text{ M}\Omega$) of reference sample. Red curve—laser is switched on. The offset current at null voltage $I(0) = -55.86\text{ nA}$ and the resistance value R is found equal to $1.0031\text{ M}\Omega$. Blue curve—the laser is switched off. $I(0) = 1.42\text{ nA}$ and $R = 1.0024\text{ M}\Omega$.

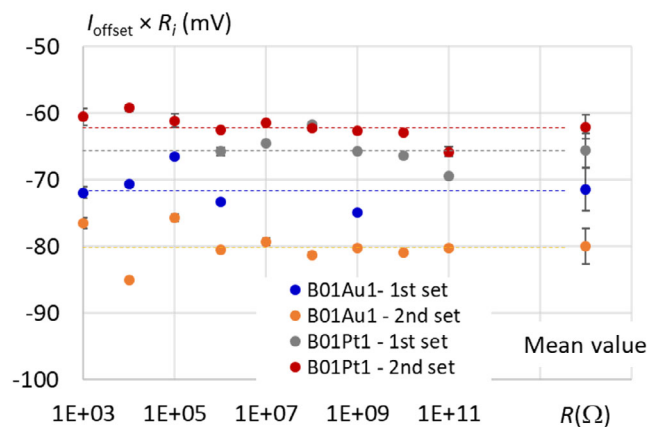


Figure 16. $I_{\text{offset}} \times R_i$ product measured on each electrode of the samples (Au electrodes sample named B01-Au1, and Pt electrodes sample named B01-Pt1) with different diamond coated tips. Mean values and corresponding standard deviations are indicated.

used for Au electrodes sample here is less opaque than that on the tip used for Pt electrodes sample. But it could just as easily be argued that the three batches of tips had comparable properties and that the difference was due to the greater reflectivity, at the wavelength used, of the Au electrodes compared with the Pt electrodes.

It is worth noting that for other kinds of conductive tip, still based on doped silicon but with metallic coatings more fragile (e.g., CrPt or PtIr tip with very small apex radius) which requires applied force lower than 500 nN , the slightest degradation (even at the tip) will illuminate the doped silicon, resulting in a photoconductive effect.

4.2.4. Discussion

From these results, it appears that both types of reference sample, fitted with Au or Pt electrodes lead to reproducible calibration of C-AFM with relatively the same accuracy. A robust and simplified uncertainty budget can also be proposed to the user, provided that three conditions are fulfilled:

Environmental Conditions:

$$\text{HR} = (40 \pm 10)\% \quad \text{and} \quad T = (23 \pm 3)^\circ\text{C} \quad (5)$$

These conditions save the user from having to apply correction on the measured values from temperature and RH effects.

AFM Tip: The use of highly doped diamond-coated tip is recommended here for covering almost all resistance range, from $100\text{ k}\Omega$ up to $1\text{ T}\Omega$. This choice relies on the robustness and the widely use of such tip in contrast with metallic tip, more fragile. The counterpart is an increased uncertainty for $100\text{ k}\Omega$ (by a factor of 10) with C-AFM operating in image mode.

However, for the smallest resistance values, i.e., ranging from $1\text{ k}\Omega$ to $10\text{ k}\Omega$, the user can consider the uncertainty value mentioned in the corresponding case only if a metallic tip is used. This is not valid for diamond tip (too resistive). Here, the deviations observed for these small resistance values are due to several effects (surface roughness, scan speed, applied force) which require deeper investigations.

Spectroscopy Mode Versus Image Mode: The use of I - V spectroscopy mode to calibrate the C-AFM is preferred, which is found more precise than the image mode and allowing to cover the complete resistance range ($1\text{ k}\Omega$ to $1\text{ T}\Omega$). The calibration of C-AFM in image mode remains possible and precise enough on a more limited resistance range, i.e., from $100\text{ k}\Omega$ and $1\text{ T}\Omega$. Simplified uncertainty budgets are presented in Table S9, Supporting Information, for the I - V mode and Table S10, Supporting Information, for the image mode. These typical uncertainty budgets are both composed of four components. The first is related to data distribution. The second uncertainty component is related to the calibration of reference sample, the

third to the environmental conditions described above, and the last one corresponds to tip resistance and concerns only the resistances lower than 1 MΩ. For the I - V mode, the uncertainty due to environmental conditions dominates the budget except for resistances $R < 1$ MΩ. The total combined uncertainty does not exceed 0.3% in the resistance range between 1 MΩ and 100 GΩ. Outside this range, the total uncertainty is estimated in the order of 1%. However for image mode, this is the standard deviation of the data distribution which becomes the major uncertainty component. As a result, the total uncertainty is larger than for I - V mode, varying between 0.5% and 1.5% for $1 \text{ M}\Omega \leq R \leq 10 \text{ G}\Omega$ and reaches 2% to 11% outside this range.

4.3. Calibration Results for DC Current Measurements

As mentioned in part 3, the C-AFM can be calibrated in terms of current amplitude by measuring the current crossing the SMD resistors or the current delivered by the SMD JFET diode at a given bias voltage. This part reports the calibration results for the C-AFM operating in spectroscopy mode performed with the JFET diode of the Pt electrodes sample and then the results obtained in image mode using SMD resistors of the Au electrodes sample.

4.3.1. Spectroscopy Mode

Considering the significant dependence of JFET diode on temperature, two series of measurements were performed: one at temperature of 22.5 °C very close to the calibration temperature (22.7 °C) and the other at 18.2 °C. The temperature sensor was placed near the sample. For these measurements, the C-AFM was fitted with a PtSi-coated tip.

Figure 17 reports the calibration results at these two temperatures and the corrected results by calculating the fit calibration curve at the measurement temperatures (18.2 °C and 22.5 °C). As expected, the significant temperature effect is observed. At temperature of 22.5 °C, the measured values deviate from the calibrated values by around -10%. After temperature correction, these deviations become less significant, lying between -8% and +4% over the full current range (100 fA to 1 μA), in respect to the total uncertainty of 2.9%. Regarding the measurements at 18.2 °C, the temperature corrections work quite well, leading to

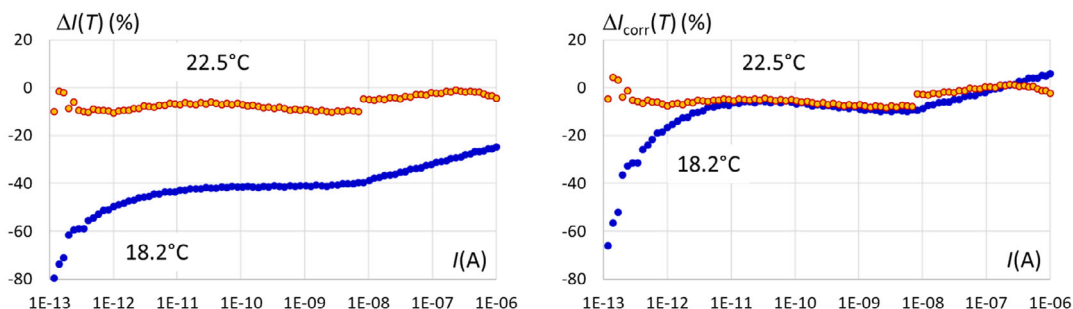


Figure 17. (Left) Relative deviations $\Delta I(T) = (I(T) - I_{\text{cal}}(T_0))/I_{\text{cal}}(T_0)$ between current values measured at a temperature T (orange: 22.5 °C, blue: 18.2 °C) and values calibrated at $T_0 = 22.7$ °C. (Right) Relative deviations $\Delta I_{\text{corr}}(T) = (I(T) - I_{\text{fit}}(T))/I_{\text{fit}}(T)$ between the measured values and the fit values calculated at the same temperature.

an agreement within -10% and +6% over a narrower current range (10 pA to 1 μA).

It is worth noting that such calibration has allowed to identify a small defect in the WCMD's automatic range change device which originates the jump at about 10 nA. This effect well pronounced at 22.5 °C is attenuated at 18.2 °C by the gradual increase in the measured current due to a probable temperature drift.

4.3.2. Image Mode

The C-AFM, here fitted with highly doped diamond coated tip, was calibrated by acquiring two images at bias voltage of +1 V and -1 V applied to the SMD resistors of the Au electrodes sample (**Figure 18**). Therefore, the delivered calibrated current values ranges from 1 pA up to 1 μA.

Figure 19 shows that the current values measured by the C-AFM agree very well with the reference values, i.e., within $\pm 1\%$, except at 1 pA for which the standard deviation is too large (52%).

Here, the total combined uncertainty is calculated from the standard deviation of data and the uncertainty related to the calibration of the sample (Table S3, Supporting Information).

It should be pointed out that this calibration carried out at fixed constant voltage is more accurate than in the case of voltage

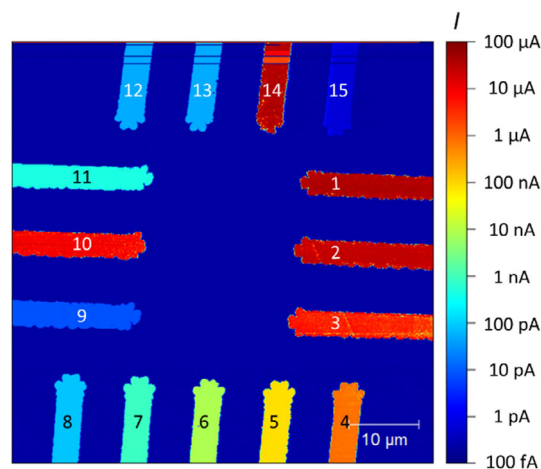


Figure 18. DC current map of the central zone of the Pt electrodes sample measured at +1 V with doped diamond-coated tip.

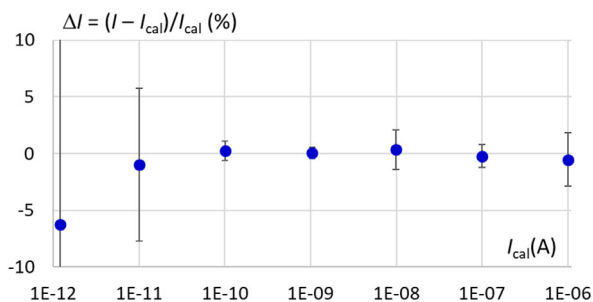


Figure 19. Relative deviations $\Delta I = (I - I_{cal}) / I_{cal}$ between current values measured with C-AFM and calibrated values from Au electrodes reference sample. The error bars represent the total combined uncertainty.

sweep more prone to errors due, for example, to the measurement device as previously reported.

4.3.3. Discussion

This last statement supported by the overall results can help the user in the choice between JFET diode and SMD resistors provided by the reference sample to calibrate their C-AFM in terms of current.

For the sake of simplicity because only one electrode is used to cover the full current range, the JFET diode will be preferred for the C-AFM calibration. Consequently, the use of tip with metallic coating will be also recommended. In this choice, the uncertainty budget is very simple to draw up since mainly governed by the uncertainty associated with the calibration of the diode. This uncertainty varies typically from 3.1% (at 10 fA) to 5.7% (1 μ A) calculated from the uncertainty corresponding to the fitted calibration curve (2.9%) and the uncertainty related to its temperature dependence. This latter ranges from 1.1% (10 fA) to 4.9% (1 μ A) provided that the room temperature remains close to 23 °C at ± 1 °C. In that case, the user will not need to correct the corresponding error term. The second and last uncertainty which might be considered (the other uncertainties being much smaller) is the standard deviation of the data distribution acquired during the C-AFM calibration. However, this uncertainty remains minor, typically limited to 0.1%.

If the user needs to calibrate the C-AFM for current measurements with the best uncertainty, then the use of electrodes connected to SMD resistors is required with no constraint on the tip materials. In this case, the total combined uncertainty remains limited to 1% for the lower part of the current range (10 fA) and can decrease down to 0.3% for the upper part (1 μ A). Here, the temperature conditions can be less restricted, $T = (23 \pm 3)$ °C, which allows the user to not apply correction on the measured values from temperature effects. The corresponding uncertainty amounts to about 0.2% for $I \geq 1$ pA and 1% for smaller current (if 1 T Ω resistor is used). The uncertainty budget remains simplified. In addition to the standard deviation of data (typically lower than 0.1%) and calibration uncertainty of SMD resistors (not exceeding 0.2%), a fourth and last uncertainty component must be considered only for high current ($I \geq 1$ nA). It is related to the tip resistance and estimated in the order of 0.1%.

5. Conclusion and Outlooks

New reference samples for calibrating resistance and current measurements by C-AFM over a very wide range of values have been developed. These samples combine SMD resistors covering 10 decades of values (from 1 k Ω to 1 T Ω), a “short-circuit” electrode designed to quantify the AFM tip resistance, and a SMD JFET diode—alone and in series with 1 and 10 G Ω resistors—offering current intensities ranging from 10 fA to 100 μ A. Operational protocols have been proposed to get the most out of these structures, and uncertainty budgets associated with the calibration of C-AFM have been established. The result is a real complete calibration kit for electrical measurements at nanoscale, the efficiency of which has been demonstrated through in-depth application to a specific example of a C-AFM device. To this end, investigations were carried out in both imaging and I - V spectroscopy modes, for two sample pad materials (Au and Pt), two probe coatings (PtSi and doped diamond), and the influence of environmental conditions was also studied.

All these elements tend to indicate that this kit could already be used as it is by any C-AFM user, just by following the recommendations given. We are, however, planning a final evolution of the reference samples, consisting of positioning all the pads connected to the various components in line. In image mode, this configuration would enable one to restrict to scanning just a few adjacent scan lines, which would drastically reduce the risk of altering/contaminating the tip apex, and would make it easier to assess the influence of applied force or scan speed. This configuration could also enable significant progress to be made in the development of an optimal image processing procedure. The new sample design will make it possible to produce series of images of a few lines sufficiently numerous to calculate resistance or current values and associated standard deviations directly from the peak values of the histograms without worrying about their shape.

In the longer term, it would be interesting to explore the calibration of electrical measurements at nanoscale in intermittent contact mode (the so-called “peak-force” or “pulsed-force”) used to study soft materials. Such an operating mode, in which the equivalent of a succession of force curves is run at a chosen cadence, would also make it possible to finely investigate the behavior of the tip/sample nanocontact and, if used on the “short-circuit” pad, would probably allow to improve the measurement of tip resistance.

6. Detailed Calibration Procedure

6.1. Foreword

For both image and spectroscopy modes, a general procedure must be followed beforehand.

First of all, it must be ensured that an electrical measurement error does not originate from the measurement device or the AFM controller. Consequently, depending on the architecture of the C-AFM device used, it may be necessary to calibrate the display and acquisition device of the AFM controller if the external inputs (input x , $\ln x$, etc.) are affected. In the latter case, the procedure consists of injecting a series of reference voltages

into the external inputs and reading the corresponding voltage on the signal profile displayed on the screen.

Do not hesitate to adjust the voltage scale on the graph to obtain maximum accuracy.

Record all the points in a table to deduce the correction factors to be applied when processing the data. For example, for the AFM controller used here, the correction formula to be applied when processing the recorded voltages is as follows: $V_{\text{actual}} = 0.99195 \times V_{\text{Controller}} - 0.00187$.

AFM will then be used to visualize the topography and electrical image of all the pads with a wide scan, which in our case will be $60 \times 60 \mu\text{m}$.

Parameters selected:

Final scan size: $60 \times 60 \mu\text{m}$

Low applied force $\approx 50\text{--}100 \text{ nN}$

Scan speed: 0.5 Hz max

Resolution: 64×64 pixels

Refocus if necessary to show all the electrodes on the image.

This step (obviously not usable for measurements) serves as a reference mark.

The following subsections detail the calibration protocol for two measurement modes: 1) Image mode for determining resistance values from a scanned surface comprising some or all of the electrodes. 2) $I\text{--}V$ spectroscopy mode, which allows resistance values to be determined from contact points chosen at each electrode.

6.2. Image Mode

Numerous comparative measurement tests, electrode by electrode, line by line, etc., have enabled us to conclude that producing a single topography and resistance image for all the electrodes, followed by postprocessing using the complete image file for each resistance electrode, gives good results. This fast procedure has the advantage of preserving the physical properties of the contact on all the electrodes in a single pass (without the risks associated with repositioning). It may be useful to acquire several images in succession so as to have several measurements taken under the same conditions on each electrode.

6.2.1. Parameters

Scan Size: $60 \times 60 \mu\text{m}$, centering the image to get all the electrodes.

Applied Force: This important parameter has a very strong influence on the quality of the contact. The applied force must depend on the nature of the tip, the local velocity during the scan, the nature of the imaged surface and, of course, the level of contamination of the surface and the degree of wear of the tip. Generally, the force to be applied: 1) should be roughly proportional to the scan speed; 2) should not exceed 500 nN for tips with a curvature radius $< 20 \text{ nm}$ (CrPt, PtIr, etc.); and 3) must not exceed $2 \mu\text{N}$ for PtSi coated tips and $3 \mu\text{N}$ for diamond coated tips.

In this work, with a scan speed of 0.5 Hz, the applied force generally was typically $1.5 \mu\text{N}$ for PtSi tips and $3 \mu\text{N}$ for diamond tips.

6.2.2. Influence of Speed and Averaging of Measurement Points on Accuracy

These two parameters are important because the quality of the value measured while the tip is moving depends not only on the local velocity but also on the number of points (measurement samples) taken into account to define the overall data to be displayed on the screen (pixel) and then recorded. Our experience of measuring all resistances from 100Ω to $1 \text{ T}\Omega$ shows that the influence of speed and averaging on accuracy is greater for low resistance values ($< 100 \text{ k}\Omega$).

During the point-by-point construction of an electrical image, the C-AFM measurement system performs a regular measurement of the current during the scanning. As the display rate of a pixel in the electrical image is generally much slower than the acquisition rate of the measurement system, the value of a pixel will be the result of an average of measured points.

As the tip moves over the surface, the measured values will vary according to the applied force, the electrical homogeneity of the material, the contamination encountered locally, and the scan speed. Parasitic resistances can therefore be added locally to the actual resistance value to be deduced at each measuring point. As a result, with the aim at measuring a minimum resistance value, some measurement points will give this minimum value, while others will give a higher value, excluding the noise of the acquisition chain.

If all the measurement points can be collected, it will then always be possible to recover, excluding the noise of the acquisition chain, the minimum values corresponding to the resistances to be measured. But if we are forced to average a set of points to make up each pixel of the electrical image, the minimum value obtained overall is likely to be higher (excluding acquisition chain noise).

This observation implies the need to minimize the number of samples to be averaged in order to achieve a minimum electrical value close to the actual value to be measured. This is particularly important for the measurement on the so-called "short-circuit" electrode (metal track with no associated SMD resistor corresponding to SC electrode in Figure 1) intended to evaluate the additional resistance (including the tip resistance), which will be subtracted from the values measured on the other electrodes. To do this, we need to know the sampling frequency of the acquisition system of the C-AFM module as well as that of the acquisition system assigned to the auxiliary inputs of the AFM controller. In this work, we are only considering the sampling frequency of the controller's auxiliary input.

Generally, in relation to its own sampling frequency, the AFM controller's imaging system will average the measured points according to the scan speed and the number of pixels chosen. Thus, for a sampling frequency of 65 535 Hz, an image resolution of 512×512 pixels and a scanning frequency of 0.5 Hz, each line (forward or reverse) lasting one second for 512 pixels, 128 measurement points will be averaged for each pixel displayed ($65\,535/512$).

The following relationship gives the number of averaged points N_{av} as a function of sampling frequency f_{sampling} and line resolution r_{line} in pixels

$$N_{\text{av}} = f_{\text{scanning}} / (2r_{\text{line}} \times f_{\text{scan}}) \quad (6)$$

It follows that to avoid averaging with the same resolution of 512 pixels would require to increase the scan speed to 64 Hz. In this work, given the size of the area scanned ($60 \times 60 \mu\text{m}$), a compromise has been found to maintain a reasonable scan speed (scan rate lower than 0.5 Hz) with few points averaged per pixel. Most of the images were produced with a resolution of 16 384 pixels per line and a scan speed of 0.3 Hz to limit local velocity (i.e., around 6 averaged points per pixel).

6.2.3. Image Acquisition Time

Acquiring a very high-resolution image requires a lot of time ($t_{\text{image}} = N_{\text{lines}}/f_{\text{scan}}$). In our case, the time spent on an image would be just over 9 h ($16\,384/0.3$ s).

There are several ways of limiting the time spent building an image: 1) Limit the number of lines, for example, by making an image of 16 384 pixels \times 1024 pixels. An option on the AFM allows one to adjust the number of lines while maintaining an aspect ratio of 1 (square image). In this work, we have chosen an image resolution of $16\,384 \times 1600$ and a scan speed of 0.3 Hz. 2) Limit the number of lines in the image by increasing the aspect ratio (rectangular image). It is then possible to maintain the same physical pitch between two successive lines as between two pixels. This solution requires the use of another type of reference sample with in-line electrodes or successive analysis of groups of in-line electrodes on the type 4A sample used here. The latter solution has also been tested with good results.

As a reminder, our various tests have shown that scanning a maximum number of electrodes during measurement ensures uniformity of the physical properties of the contact across all the electrodes.

6.3. Spectroscopy Mode

I-*V* curves measurements are carried out by leaving the tip at a chosen point on the surface of each electrode. Finding a point on the surface that is as conductive as possible before taking the *I*-*V* measurement sometimes requires a great deal of time and determination, especially when measuring resistances of less than 100 k Ω . The protocol is composed of the following steps:

a) Set the C-AFM measuring device to continuous resistance (or current) measurement mode.

b) Initially, try to use AFM to visualize the topography and electrical image of all the electrodes with a wide scan. The selected parameters are: 1) scan Size: $60 \times 60 \mu\text{m}$, 2) low applied force, i.e., typically between 50 nN and 100 nN, 3) scan speed limited to 0.5 Hz at most, and 4) resolution: 64×64 pixels.

Refocus if necessary to show all the electrodes on the image.

c) Locate the electrode to be measured on the image.

d) Center the image in the middle of this electrode (use the "offset" button) and reduce the scan size so as to obtain an image centered on the electrode with the outside of the electrode on either side of the image. Adjust the scan angle so that the scan is perpendicular to the electrode axis. For the reference sample used here, the ideal scan size is $8 \mu\text{m}$.

e) Increase the resolution to 256 pixels.

f) Increase the contact force to around 500 nN.

Modifying these last two parameters should make it easier to observe variations in resistance (or current), particularly at the two edges of the electrode.

g) Center the scan on the middle of a well-conducted area and reduce the scan size while remaining centered on the conductive area.

Repeat the above steps if electrical contact is lost and look again for a conductive area by increasing the scan size.

h) If the conduction level is ideal, with a minimum resistance profile (or maximum current profile) over a good part of the screen, set the "Slow Scan Axis" option to "Disabled" to keep the scan on the same line.

i) Increase the contact force to try to reduce the resistance value level even further while not exceeding the maximum force values as afore mentioned.

Repeat the above steps if contact is lost by increasing the scan size again, adjusting the force applied and setting the "Slow Scan Axis" option back to "Enabled".

Finally, with a scan size lower than 5 nm, we need to obtain a resistance profile that is as low as possible (or as maximum as possible for current), even across the width of the screen and clean.

j) At this point, start the *I*-*V* measurement.

Supporting Information

Supporting Information is available from the Wiley Online Library or from the author.

Acknowledgements

The authors are grateful to Khaled Kaja for his critical reading and comments. This research work was carried out in the framework of the ELENA project (EMPIR 20IND12), which was supported by the European Metrology Programme for Innovation and Research (EMPIR). The EMPIR initiative was cofunded by the European Horizon 2020 research and innovation program and the EMPIR Participating States. Part of this work was done at the C2N micro nanotechnologies platforms and was partly supported by the RENATECH network and the General Council of Essonne.

Conflict of Interest

The authors declare no conflict of interest.

Data Availability Statement

The data that support the findings of this study are available from the corresponding author upon reasonable request.

Keywords

calibration, conductive probe atomic force microscope, currents, measurement protocols, nanoscale, reference samples, resistance

Received: September 3, 2024

Revised: November 20, 2024

Published online:

- [1] M. Lanza, in *Conductive Atomic Force Microscopy: Applications in Nanomaterials*, Wiley-VCH, Weinheim, Germany **2017**.
- [2] S. V. Kalinin, A. Gruverman, in *Introduction Scanning Probe Microscopy Techniques for Electrical and Electromechanical Characterization. Scanning Probe Microscopy*, Vol.1, Springer, New York, NY **2007**, pp 1–8.
- [3] M. P. Murrell, M. E. Welland, S. J. O’Shea, T. M. H. Wong, J. R. Barnes, A. W. McKinnon, M. Heyns, S. Verhaverbeke, *Appl. Phys. Lett.* **1993**, 62, 786.
- [4] W. Vandervorst, M. Meuris, *U.S. Patent US5369372A*, **1994**.
- [5] S. J. O’Shea, R. M. Atta, M. P. Murrell, M. E. Welland, *J. Vac. Sci. Technol. B* **1995**, 13, 1945.
- [6] P. De Wolf, *J. Vac. Sci. Technol. B*, **1998**, 16, 355.
- [7] O. Schneegans, P. Chrétien, F. Houzé, *WO Pat. Appl. WO2011138738A1*, **2011**.
- [8] O. Schneegans, P. Chrétien, F. Houzé, *Eur. Pat. Appl. EP2567245A1*, **2013**.
- [9] L. Jiang, J. Weber, F. M. Puglisi, P. Pavan, L. Larcher, W. Frammelsberger, G. Benstetter, M. Lanza, *Materials* **2019**, 12, 459.
- [10] S. A. Sumaiya, A. Martini, M. Z. Baykara, *Nano Express* **2020**, 1, 030023.
- [11] M. R. Vazirisereshk, S. A. Sumaiya, R. Chen, M. Z. Baykara, A. Martini, *Tribol. Lett.* **2021**, 69, 50.
- [12] J. Weber, Y. Yuan, F. Kühnel, C. Metzke, J. Schätz, W. Frammelsberger, G. Benstetter, M. Lanza, *ACS Appl. Mater. Interfaces* **2023**, 15, 21602.
- [13] F. Piquemal, K. Kaja, P. Chrétien, J. Morán-Meza, F. Houzé, C. Ulysse, A. Harouri, *Beilstein J. Nanotechnol.* **2023**, 14, 1141.
- [14] Joint Committee for Guides in Metrology – JCGM, *Evaluation of Measurement Data—Guide to the Expression of Uncertainty in Measurement. JCGM 100*, **2008**.